

Investigation of rat breast tumour oxygen consumption by near-infrared spectroscopy

Yulin Song^{1,2}, Jae G Kim¹, Ralph P Mason² and Hanli Liu^{1,3}

¹ Joint Graduate Program in Biomedical Engineering, University of Texas at Arlington/University of Texas Southwestern Medical Center at Dallas, Arlington, TX 76019, USA

² Advanced Radiological Sciences, Department of Radiology, University of Texas Southwestern Medical Center at Dallas, Dallas, TX 75390, USA

E-mail: hanli@uta.edu

Received 5 December 2004, in final form 2 March 2005

Published 22 July 2005

Online at stacks.iop.org/JPhysD/38/2682

Abstract

This study develops a mathematical model for calculating the tumour oxygen consumption rate and investigates the correlation with tumour volume. Near-infrared spectroscopy (NIRS) was used to measure changes of oxygenated haemoglobin concentration ($\Delta[\text{HbO}_2]$) before and after potassium chloride (KCl) induced cardiac arrest. Measurements were made in five 13762NF mammary adenocarcinomas implanted in female adult Fisher 344 rats, while the anaesthetized rats breathed air. After 5–10 min of baseline NIRS measurement, KCl overdose was administered intravenously in the tail. NIRS showed a significant drop in tumour vascular oxygenation immediately following KCl induced cardiac arrest. The tumour oxygen consumption rate was calculated by fitting the model to the measured $\Delta[\text{HbO}_2]$ data, and a relationship between the tumour oxygen consumption rate and tumour volume was analysed using linear regression. A strong negative linear relationship was found between the mean tumour oxygen consumption rate and tumour volume. This study demonstrates that the NIRS can provide an efficient and real-time approach to quantify tumour oxygen consumption rate, while further development is required to make it non-invasive.

1. Introduction

The physiology of solid tumours is highly complex and largely associated with multiple physiological parameters, such as tumour blood flow, blood volume, blood oxygen saturation, tissue oxygen tension ($p\text{O}_2$) and oxygen consumption. It is known that tumour microvasculature is often abnormal, leaky and having distended capillaries and sluggish flow [1–3]. Hypoxic regions exist in almost all solid tumours, and tumour oxygenation greatly affects tumour growth, malignant progressions, tumour prognosis and therapy efficacy. Therefore, understanding the various physiological

parameters of solid tumours is significant for better strategies and efficacy in treating solid tumours in the near future.

Over the past decade, substantial studies have been conducted in both laboratory and clinical settings to non-invasively investigate tissue/tumour vascular oxygenation [4–8] and blood flow [9, 10] using near-infrared (NIR) spectroscopy (NIRS) and imaging. Several studies were also reported on tumour $p\text{O}_2$ heterogeneity [11] and on comparisons between tumour vascular oxygenation and tumour $p\text{O}_2$ using animal tumour models during hyperoxic gas interventions [12, 13]. Regarding tissue oxygen consumption, considerable efforts have been made in developing techniques for measuring skeletal muscle oxygen consumption ($\dot{V}\text{O}_2$) during rest and exercise with and without vascular occlusion [14–18]. More recently,

³ Author to whom any correspondence should be addressed.

extensive attention has been paid to quantitative relationships among neuronal activity, oxygen metabolism and haemodynamic responses [19–22]. While various mathematical models for computing or interpreting haemoglobin concentrations have been proposed [23–25], the approaches for calculations of oxygen consumptions in human muscles versus in the brain during cortical activation are quite diversified.

In principle, tumour oxygen consumption is quite different from regular muscle or brain oxygen consumptions, which warrants separate studies targeting on tumour oxygen consumption. In this regard, little is known about tumour oxygen consumption even in animal models, or its relationship to tumour kinetic parameters and tumour volume. Some earlier studies indicated that oxygen consumption rates of breast tumours *in vivo* were intermediate between normal tissues with low metabolic rates and normal tissues with quite high activities [26]. Steen *et al* [27] found out that the oxygen consumption rate of the rat brain was higher than that of 9L gliosarcoma by comparing pre-sacrifice and post-sacrifice sO_2 (haemoglobin oxygen saturation) values. While a few reports recently appeared in the literature on determination of the tumour oxygen consumption rate through *in vitro* measurements using a standard Clark-type oxygen electrode [10, 28], overall knowledge and investigation on tumour oxygen consumption is still limited and much needed.

It would be desirable to develop a non-invasive technique or methodology to quantify tumour oxygen consumption rate; however, it would be still acceptable to conduct invasive studies if significant knowledge on tumour oxygen consumption can be explored. In this paper, we report a novel methodology to quantify the tumour oxygen consumption rate using an invasive approach, to be done by the end of regular tumour experiments when the animals had to be sacrificed. In the experiment, we took the NIR readings from the animal tumours during potassium chloride (KCl) induced cardiac arrest (total global ischemia), as a procedure for animal euthanasia. In theory, we have developed a simple mathematical model based on Fick's Law of diffusion to describe haemokinetics of tumour vascular oxygenated haemoglobin concentration $[HbO_2]$. The model describes changes in tumour oxyhaemoglobin concentration $\Delta[HbO_2]$, as a function of time. Specifically, the mathematical model is developed in such a way that the measured $\Delta[HbO_2]$ is directly associated with the tumour oxygen consumption rate, which can be further correlated with the tumour volume. In this paper, we will report (1) $\Delta[HbO_2]$ measurement using NIRS from the animal tumour models, in common with our previous work [12, 29], (2) the development of the mathematical model for computing the tumour oxygen consumption rate and (3) the investigation of the relationship between the tumour oxygen consumption rate and tumour volume.

2. Materials and methods

2.1. Calculations of tumour $[HbO_2]$ and $[Hb]_{total}$

The principle of tissue NIRS is that concentrations of oxygenated haemoglobin $[HbO_2]$ and deoxygenated haemoglobin $[Hb]$, respectively, are the only significant absorbing materials in the tissue within the NIR range (700–900 nm). When the measured sample, such as a tumour,

has a mixture of oxygenated and deoxygenated haemoglobin, the modified Beer–Lambert law can be written as [30–32]

$$OD^\lambda = \{\varepsilon_{Hb}^\lambda [Hb] + \varepsilon_{HbO_2}^\lambda [HbO_2]\}l, \quad (1)$$

where OD^λ is the optical density or absorbance at wavelength λ , ε_{Hb}^λ and $\varepsilon_{HbO_2}^\lambda$ are the extinction coefficients at λ for molar concentrations of $[Hb]$ and $[HbO_2]$, respectively and l is the optical path length. By employing two wavelengths at λ_1 and λ_2 , both $[HbO_2]$ and $[Hb]$ can be determined by measuring the light absorbance at the two specific wavelengths provided that the values for ε_{Hb}^λ and $\varepsilon_{HbO_2}^\lambda$ are known:

$$[HbO_2] = \frac{\varepsilon_{Hb}^{\lambda_2} OD^{\lambda_1} - \varepsilon_{Hb}^{\lambda_1} OD^{\lambda_2}}{l(\varepsilon_{Hb}^{\lambda_2} \varepsilon_{HbO_2}^{\lambda_1} - \varepsilon_{Hb}^{\lambda_1} \varepsilon_{HbO_2}^{\lambda_2})}, \quad (2)$$

$$[Hb] = \frac{\varepsilon_{HbO_2}^{\lambda_2} OD^{\lambda_1} - \varepsilon_{HbO_2}^{\lambda_1} OD^{\lambda_2}}{l(\varepsilon_{Hb}^{\lambda_1} \varepsilon_{HbO_2}^{\lambda_2} - \varepsilon_{Hb}^{\lambda_2} \varepsilon_{HbO_2}^{\lambda_1})}. \quad (3)$$

It follows that changes in $[Hb]$ and $[HbO_2]$ are given by:

$$\Delta[HbO_2] = \frac{\varepsilon_{Hb}^{\lambda_2} \Delta OD^{\lambda_1} - \varepsilon_{Hb}^{\lambda_1} \Delta OD^{\lambda_2}}{l(\varepsilon_{Hb}^{\lambda_2} \varepsilon_{HbO_2}^{\lambda_1} - \varepsilon_{Hb}^{\lambda_1} \varepsilon_{HbO_2}^{\lambda_2})}, \quad (4)$$

$$\Delta[Hb] = \frac{\varepsilon_{HbO_2}^{\lambda_2} \Delta OD^{\lambda_1} - \varepsilon_{HbO_2}^{\lambda_1} \Delta OD^{\lambda_2}}{l(\varepsilon_{Hb}^{\lambda_1} \varepsilon_{HbO_2}^{\lambda_2} - \varepsilon_{Hb}^{\lambda_2} \varepsilon_{HbO_2}^{\lambda_1})}, \quad (5)$$

where ΔOD^λ represents a change in optical density at the specific wavelength, λ and equals $\log(A_B/A_T)$. A_B and A_T correspond to light intensities measured under the baseline and transient conditions.

Equations (4) and (5) seem straightforward mathematically and have been used for several decades by biochemists to quantify $\Delta[Hb]$ and $\Delta[HbO_2]$ in laboratory spectrophotometric measurements. However, close attention needs to be paid to the values of ε for *in vivo* haemoglobin determination, since ε values were often expressed on a basis of per haeme whereas the haemoglobin molecule has four haemes. Therefore, there exists a factor of 4 between the commonly published ε values and the ε values to be used in equations (4) and (5) for *in vivo* measurements [33, 34]. Furthermore, the optical pathlength, l , should be proportional to the source and detector separation, d , with a differential pathlength factor (DPF) [35, 36], i.e. $l = d \times DPF$. We previously utilized the ε values given by Zijlstra *et al* [37] which were expressed on a haeme basis and assumed that the DPF values were constant at the two wavelengths. For $\lambda_1 = 758$ nm and $\lambda_2 = 785$ nm, equations (4) and (5) gave the following empirical relationships based on system calibration using liquid phantoms [12]:

$$\begin{aligned} \Delta[HbO_2] &= \frac{-10.63 \cdot \log(A_B/A_T)^{758} + 14.97 \cdot \log(A_B/A_T)^{785}}{d}, \end{aligned} \quad (6)$$

$$\Delta[Hb] = \frac{8.95 \cdot \log(A_B/A_T)^{758} - 6.73 \cdot \log(A_B/A_T)^{785}}{d}, \quad (7)$$

$$\begin{aligned} \Delta[Hb]_{total} &= \Delta[Hb] + \Delta[HbO_2] \\ &= \frac{-1.68 \cdot \log(A_B/A_T)^{758} + 8.24 \cdot \log(A_B/A_T)^{785}}{d}. \end{aligned} \quad (8)$$

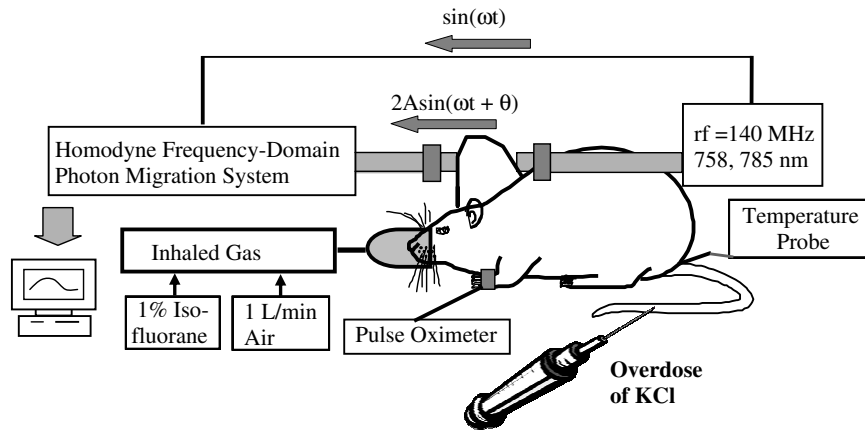


Figure 1. Schematic set-up of one-channel, NIR, frequency domain IQ instrument for tumour investigation *in vivo*. Two fibre bundles were used to deliver and detect the laser light, at 758 and 785 nm, which were transmitted through the implanted tumour. The overdose of KCl was administered by tail vein injection after 5–10 min of $\Delta[\text{HbO}_2]$ baseline measurement.

The factor 4 in ε relating to 4 haemes and the DPF values are essentially constants and do not affect the dynamic features of the tumour $\Delta[\text{HbO}_2]$. For simplicity, thus, we did not include them in these equations and used arbitrary units for $\Delta[\text{Hb}]$ and $\Delta[\text{HbO}_2]$ since the focus of this study is on relative changes of $\Delta[\text{HbO}_2]$ between the baseline conditions and response to KCl injection. The error estimation due to the assumption of constant DPF has been given in [29].

2.2. One-channel NIRS system

A dual-wavelength (at 758 and 785 nm), one-channel NIR system (NIM Inc., Philadelphia, PA) was used (figure 1). A radiofrequency (RF) source was used to modulate the light intensities of two laser diodes at 140 MHz through a time-sharing system. After the light passed through a bifurcated fibre optic probe, it was transmitted through the tumour tissue and then collected by a second fibre bundle. The light was demodulated by an in-phase and quadrature-phase chip (I&Q chip), amplified by a photo multiplier tube (PMT) and filtered by a low pass (LP) filter to pass only the dc electronic components. The signals were digitized by an analog-to-digital converter (ADC) and stored in a laptop computer. The I&Q chip served as a frequency mixer, giving high and low (near dc) components. The measured dc electrical signals at the *I* and *Q* branches, $I_{\text{DC}}(\lambda)$ and $Q_{\text{DC}}(\lambda)$, contained the quantities of optical amplitudes, $A(\lambda)$, and phase, $\theta(\lambda)$, that passed through the tumour tissues [38]. Both $A(\lambda)$ and $\theta(\lambda)$ can be recovered through the dc output readings at the *I* and *Q* branches, as

$$A(\lambda) = \sqrt{I(\lambda)_{\text{DC}}^2 + Q(\lambda)_{\text{DC}}^2}, \quad (9a)$$

$$\theta(\lambda) = \tan^{-1} \left(\frac{Q(\lambda)_{\text{DC}}}{I(\lambda)_{\text{DC}}} \right), \quad (9b)$$

where λ represents the respective wavelengths utilized in the NIR system. Although our NIR system allowed us to quantify both the amplitudes and phase, the phase information was not utilized in the study. The reasons for abandoning $\theta(\lambda)$ are that (1) the diffusion theory was not valid for use in this case due to

the finite size and heterogeneity of solid tumours, and (2) only the modified Beer–Lambert law was applied for the calculation. In the calculation, we employed only the measured values of $A(\lambda)$ at the two selected wavelengths and substituted them in equations (6)–(8) to compute changes in tumour vascular $[\text{HbO}_2]$ and $[\text{Hb}]_{\text{total}}$.

2.3. Animal tumour model and its response to KCl injection

Rat mammary adenocarcinomas 13762NF were implanted in skin pedicles on the forebacks of adult female Fischer 344 rats (~ 250 g, $n = 5$), as described in detail previously [39]. Relatively large tumours (~ 1.2 – 1.5 cm in radius or ~ 7 – 14 cm³ in tumour volume) were used to ensure that the NIRS interrogated only the tumour tissue rather than the surrounding normal skin tissue. The rats were anaesthetized with 200 μ l ketamine hydrochloride intraperitoneal (100 mg ml⁻¹; Aveco, Fort Dodge, IA) and maintained under general gaseous anaesthesia with air (1.0 litre min⁻¹) and 1.0% isoflurane. Hair around the tumours was cut with scissors to improve the NIR light transmission and the three orthogonal diameters were measured by caliper to estimate tumour volume. The rats were placed on their sides in an animal bed and stabilized using tape to reduce potential motion artefacts caused by breathing movements. The body temperature was maintained at about 37°C by a warm water blanket connected to a water pump (K-MOD 100, Baxter Healthcare Co., Deerfield, IL). A fibre optic pulse oximeter (Nonin Medical Inc., Plymouth, MN) was placed on the front foot to monitor arterial haemoglobin saturation ($s_a\text{O}_2$) and heart rate (HR), and a thermocouple (Cole-Parmer Instrument Co., Vernon Hills, IL) was inserted rectally to monitor core temperature (figure 1).

Following baseline $\Delta[\text{HbO}_2]$ measurement (5–10 min), while the rats were breathing air, they were given an overdose of KCl (1 g kg⁻¹ in saline) i.v. in the tail. Without disturbing the position of the light source, detector or tumour, the changes in the tumour vascular $[\text{HbO}_2]$ and total haemoglobin concentration ($[\text{Hb}]_{\text{total}}$) were continuously monitored during and after cardiac arrest for about 40 min by NIRS.

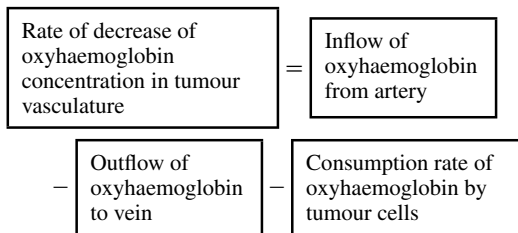
2.4. Data analysis

Raw data were filtered, baseline corrected and fitted to the mathematical model (described below) to determine the kinetic parameters of the dynamic response. Tumour oxygen consumption rate $\dot{V}O_2$ and mean tumour oxygen consumption rate $\bar{V}O_2$ were computed for five rat tumours, respectively, by fitting the mathematical model with the measured $\Delta[\text{HbO}_2]$. Relationships between those parameters and tumour volume were analysed using linear regression.

3. Development of a mathematical model for tumour oxygen consumption rate

3.1. Dynamic changes of tumour $[\text{HbO}_2]$ caused by KCl injection

We previously [29] applied Kety's approach [40] to evaluate tumour haemodynamics by using HbO_2 intervention as a tracer, but we did not consider the effect of tumour oxygen consumption. In this study, we included the tumour oxygen consumption rate in our haemodynamic model. In principle, the rate of change of HbO_2 in tumour vasculature should be equal to the rate at which the HbO_2 is transported in by arterial circulation minus the rate at which it is carried away into the venous drainage and minus the rate at which tumour cells consume oxygen. In common with our previous approach [29], we assumed a one-compartment model: tumour vasculature is well mixed with respect to oxygen so that a mass balance equation for HbO_2 can be written by the following chart. Specifically, if $[\text{HbO}_2]$ is the oxyhaemoglobin concentration in the tumour at a given time t , the general conservation of mass equation for $[\text{HbO}_2]$ can be schematically depicted as:



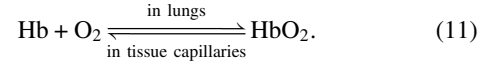
By using Fick's law of diffusion, the above schematic diagram can be written mathematically as

$$\frac{d[\text{HbO}_2]}{dt} = f \cdot [\text{HbO}_2]_A - f \cdot [\text{HbO}_2]_V - \kappa \cdot [\text{HbO}_2], \quad (10)$$

where $[\text{HbO}_2] = [\text{HbO}_2](t)$ (arbitrary unit) is a solution to this differential equation and is a function only of time. Because of the one-compartment model, f is the blood perfusion rate ($\text{ml min}^{-1} \text{cm}^{-3}_{\text{tissue}}$), $[\text{HbO}_2]_A$ and $[\text{HbO}_2]_V$ are oxyhaemoglobin concentrations in the arterial and venous blood in the tumour, respectively and κ is defined as the oxyhaemoglobin dissociation constant (min^{-1}).

In equation (10), we assumed that the oxyhaemoglobin dissociation rate is equal to the tumour oxygen consumption rate at the steady state. This assumption is based on the following: deoxyhaemoglobin and oxygen molecules normally combine to form oxyhaemoglobin through a loading reaction that occurs in the lungs. Oxyhaemoglobin, in turn, can be

dissociated to deoxyhaemoglobin and free oxygen molecules through an unloading process that occurs in the tissue capillaries. These two processes can be expressed as the reversible reaction



The direction of the reaction depends largely on two factors: (1) the $p\text{O}_2$ of the environment and (2) the affinity of haemoglobin for oxygen. A high $p\text{O}_2$ drives the equation to the right promoting oxygen loading, whereas low $p\text{O}_2$ in the tissue capillaries drives the reaction to the left to promote oxygen unloading. The affinity of haemoglobin for oxygen does not change appreciably over a short period of time (minutes). Since the rat died rapidly by KCl-induced cardiac arrest, the reaction went to the left to unload oxygen because of lack of oxygen supply from incoming blood. The oxygen dissolved in the plasma and diffused to the surrounding tumour tissues, where it was consumed by aerobic cellular respiration.

Assuming that the rat died instantaneously by KCl-induced cardiac arrest, then the blood flow stopped, the lungs no longer functioned and the gas exchange between the alveolar air and the blood in pulmonary capillaries ceased. As a result, no further oxyhaemoglobin molecules were transported either to or from the tumour vasculature. Mathematically, this means that the tumour blood perfusion rate f is 0 after KCl administration. Equation (10), therefore, simplifies to

$$\frac{d[\text{HbO}_2]}{dt} = -\kappa \cdot [\text{HbO}_2]. \quad (12)$$

To solve equation (12), we need to know its initial condition, which is given by

$$[\text{HbO}_2]_{t=0} = [\text{HbO}_2]_0, \quad (13)$$

where $[\text{HbO}_2]_0$ is the initial baseline value (pre-KCl administration) of oxyhaemoglobin concentration. Rearranging and integrating equation (12) gives rise to an exponential solution

$$\int \frac{d[\text{HbO}_2]}{[\text{HbO}_2]} = - \int \kappa dt \Rightarrow [\text{HbO}_2](t) = C \cdot e^{-\kappa t}, \quad (14)$$

where C is the constant of integration. By applying the initial condition, equation (13), we obtain the solution as follows:

$$[\text{HbO}_2](t) = [\text{HbO}_2]_0 \cdot e^{-\kappa t}. \quad (15)$$

Equation (15) indicates that following KCl-induced cardiac arrest, tumour vascular $[\text{HbO}_2]$ decreases exponentially with time and this process is characterized by the dissociation constant κ and the initial oxyhaemoglobin concentration $[\text{HbO}_2]_0$, both of which can be determined by fitting equation (15) to the experimental data.

Furthermore, it is useful to introduce the mean lifetime τ , defined as the average time that an oxyhaemoglobin molecule is likely to survive before it is dissociated from oxygen. The number of oxyhaemoglobin molecules that survive to time t is $[\text{HbO}_2](t)$ and the number of oxyhaemoglobin molecules that dissociate between t and $t + dt$ is $|d[\text{HbO}_2]/dt| \cdot dt$. Thus, the theoretical mean lifetime τ is

$$\tau = \frac{\int_0^\infty t \cdot |d[\text{HbO}_2]/dt| \cdot dt}{\int_0^\infty |d[\text{HbO}_2]/dt| \cdot dt}, \quad (16)$$

where $\int_0^\infty |d[\text{HbO}_2]/dt| \cdot dt$ gives the total number of oxyhaemoglobin molecules that are dissociated after KCl administration and $\int_0^\infty |d[\text{HbO}_2]/dt| \cdot dt$ is equal to $[\text{HbO}_2]_0$. Evaluating equation (16) gives

$$\begin{aligned} \tau &= \frac{\int_0^\infty t \cdot [\text{HbO}_2]_0 \cdot (-\kappa) \cdot e^{-\kappa t} \cdot dt}{\int_0^\infty [\text{HbO}_2]_0 \cdot (-\kappa) \cdot e^{-\kappa t} \cdot dt} \\ &= \frac{1/\kappa \int_0^\infty (\kappa t) \cdot e^{-\kappa t} \cdot d(\kappa t)}{\int_0^\infty e^{-\kappa t} \cdot d(\kappa t)} = \frac{1}{\kappa}. \end{aligned} \quad (17)$$

Equation (17) indicates that the mean lifetime τ is simply the inverse of the dissociation constant κ and is just the time constant of equation (15), which, therefore, can be rewritten as

$$[\text{HbO}_2](t) = [\text{HbO}_2]_0 \cdot e^{-t/\tau}. \quad (18)$$

Since we only measure relative changes of $[\text{HbO}_2]$, we can express $\Delta[\text{HbO}_2]$ as

$$\Delta[\text{HbO}_2] = [\text{HbO}_2] - [\text{HbO}_2]_0 = -[\text{HbO}_2]_0(1 - e^{-t/\tau}). \quad (19)$$

In this way, both quantities of $[\text{HbO}_2]_0$ and τ can be obtained by fitting equation (19) with the experimental data taken from the changes in $[\text{HbO}_2]$ caused by KCl-induced cardiac arrest. As seen from this equation, when the measuring time is long, i.e. $t \rightarrow \infty$, the stabilized $\Delta[\text{HbO}_2]$ reaches the value of $[\text{HbO}_2]_0$.

3.2. Tumour oxygen consumption rate $\dot{V}\text{O}_2$

It is perhaps more important and significant to compute the tumour oxygen consumption rate $\dot{V}\text{O}_2$ from $\Delta[\text{HbO}_2]$, because it reflects tumour oxygen consumption and metabolic activities. Tumour oxygen consumption rate $\dot{V}\text{O}_2$ is determined by taking the first order derivative of equation (15) with respect to time t ,

$$\begin{aligned} |\dot{V}\text{O}_2(t)| &= \left| \frac{d}{dt} [[\text{HbO}_2]_0 \cdot e^{-t/\tau}] \right| = \left| -\frac{[\text{HbO}_2]_0}{\tau} \cdot e^{-t/\tau} \right| \\ &= \left| -\frac{[\text{HbO}_2](t)}{\tau} \right|, \end{aligned} \quad (20)$$

which reflects the number of oxyhaemoglobin molecules that are dissociated per unit time at a particular time t . The 'minus' sign reflects the opposite direction between a decrease in $[\text{HbO}_2](t)$ and an increase in $\dot{V}\text{O}_2(t)$. This equation shows that the tumour oxygen consumption is proportional to the concentration of $[\text{HbO}_2]$ in our experimental case in an opposite direction. In particular, equation (20) permits direct quantification of the regular tumour oxygen consumption rate, $\dot{V}\text{O}_2(t=0)$ as being $[\text{HbO}_2]_0/\tau$, which can be obtained by fitting equation (19) to our experimental data. Furthermore, taking the logarithm of equation (20) leads to

$$\ln|\dot{V}\text{O}_2| = \frac{-t}{\tau} + \ln|\dot{V}\text{O}_2(t=0)|, \quad (21)$$

where $\dot{V}\text{O}_2$ has been taken as an absolute value to obtain logarithmic expressions. This equation demonstrates a linear relationship between the logarithm of magnitude of the tumour oxygen consumption rate and time after the KCl injection with a slope being the inverse of the time constant of $\Delta[\text{HbO}_2]$ decay following cardiac arrest.

To facilitate the comparison of the tumour oxygen consumption rates as a function of tumour volume, we also computed an absolute value of mean tumour oxygen consumption rate as follows:

$$|\bar{V}\text{O}_2| = \frac{1}{T} \int_0^T \frac{[\text{HbO}_2]_0}{\tau} \cdot e^{-t/\tau} dt, \quad (22)$$

where T is the time that it takes for oxyhaemoglobin concentration to drop to a steady or asymptotic minimum value. In order to evaluate the integral, we made an approximation: $T = 3\tau$ because the tumour oxyhaemoglobin concentration dropped to 5% of its initial value within 3τ , and the error introduced by this approximation was minimal. Evaluating equation (22) with $T = 3\tau$ gives

$$|\bar{V}\text{O}_2| = \frac{1}{3\tau} \int_0^{3\tau} \frac{[\text{HbO}_2]_0}{\tau} \cdot e^{-t/\tau} dt \approx \frac{1}{3} \left(\frac{[\text{HbO}_2]_0}{\tau} \right). \quad (23)$$

Both equations (20) and (23) indicate that the quantity $([\text{HbO}_2]_0/\tau)$ has an important physiological significance, representing the transient and mean tumour oxygen consumption rate and reflecting the metabolic activity of the tumour.

4. Experimental results

Figure 2(a) shows the KCl effects on tumour vascular $\Delta[\text{HbO}_2]$ and $\Delta[\text{Hb}]_{\text{total}}$ for a representative mammary adenocarcinoma 13762NF (12.7 cm³). The exponential appearance of the curve matches the solution to the mathematical model, equation (19) and $\Delta[\text{HbO}_2]$ dropped sharply and significantly by 0.8723 ± 0.0002 ($p < 0.0001$). In contrast total haemoglobin concentration, $[\text{Hb}]_{\text{total}}$, decreased by 0.0870 ± 0.0001 , only 10% of the change in $[\text{HbO}_2]$. This indicates that total tumour blood volume remained relatively constant, when compared to $[\text{HbO}_2]$ during the course of the experiment. This also shows that the assumption of blood flow $f = 0$ after the KCl injection was reasonable. By fitting equation (19) to the data, $[\text{HbO}_2]_0$ and τ were found to be 0.880 ± 0.005 and 0.691 ± 0.004 min, respectively. Figure 2(b) shows the time course profiles of tumour vascular $\Delta[\text{HbO}_2]$ and $\Delta[\text{Hb}]_{\text{total}}$ for a second tumour (15.7 cm³). In this case, $\Delta[\text{HbO}_2]$ dropped by 1.444 ± 0.005 ($p < 0.0001$), while $\Delta[\text{Hb}]_{\text{total}}$ dropped by 0.488 ± 0.002 . As for the first breast tumour, the magnitude of the drop in $\Delta[\text{Hb}]_{\text{total}}$ was much less than that in $\Delta[\text{HbO}_2]$. The values of $[\text{HbO}_2]_0$ and τ were determined as 1.192 ± 0.008 min and 1.36 ± 0.02 min, respectively, based on equation (19). For the five tumours, a strong linear relationship was found between tumour $[\text{HbO}_2]_0$ and tumour volume (figure 3) and between the mean lifetime (τ) and tumour volume (figure 4).

Figure 5 shows the relationships between the tumour oxygen consumption rates, $\dot{V}\text{O}_2$, as a function of time and tumour volume. To better separate the curves, the data only for the first 4 min after the KCl injection were plotted. Each curve was obtained by substituting corresponding $[\text{HbO}_2]_0$ and τ values to equation (20). The same relationships were replotted in figure 6 on a semilog graph, giving straight lines of slope $1/\tau$ according to equation (21). From these two figures, it appeared that smaller tumours had greater oxygen consumption rates before and right after the KCl injection. It is more significant and important to be able to estimate the

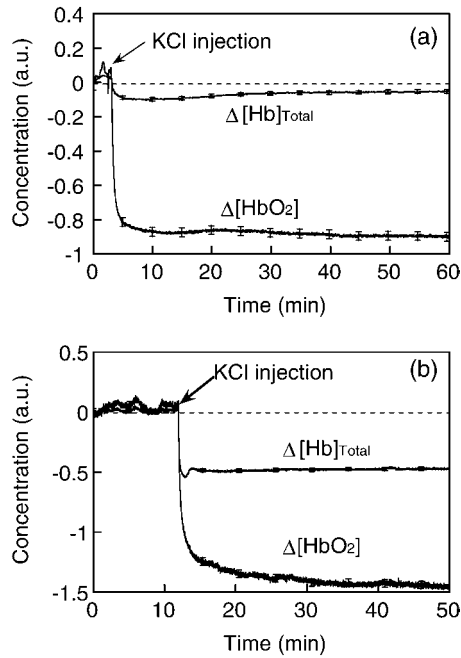


Figure 2. Effects of overdose KCl injection on tumour vascular $\Delta[\text{HbO}_2]$ and $\Delta[\text{Hb}]_{\text{total}}$ for two breast tumours: (a) 12.7 cm^3 and (b) 15.7 cm^3 . $\Delta[\text{HbO}_2]$ dropped rapidly and significantly ($p < 0.0001$). Both $\Delta[\text{HbO}_2]$ and $\Delta[\text{Hb}]_{\text{total}}$ are in arbitrary units. The error bars indicate measurement uncertainties and are labelled at selected locations. (Some of them are too small to be seen.)

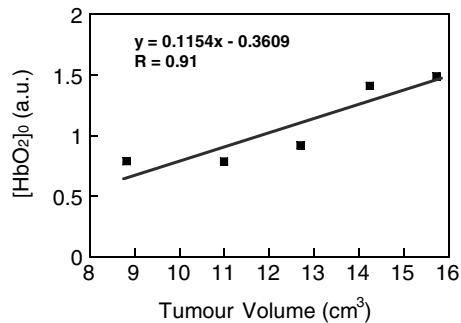


Figure 3. Relationship between tumour $[\text{HbO}_2]_0$ and tumour volume for five mammary adenocarcinomas 13762NF.

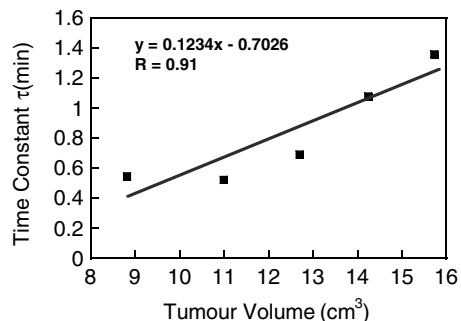


Figure 4. Relationship between time constant τ and tumour volume for five mammary adenocarcinomas 13762NF.

tumour oxygen consumption rate when the rats were alive. Considering that the rats were alive at $t = 0$, $\dot{V}\text{O}_2$ (alive) was determined by setting $t = 0$ in equation (20). Thus, $\dot{V}\text{O}_2(\text{alive}) = \dot{V}\text{O}_2(t = 0) = [\text{HbO}_2]_0/\tau$. Figure 7 shows

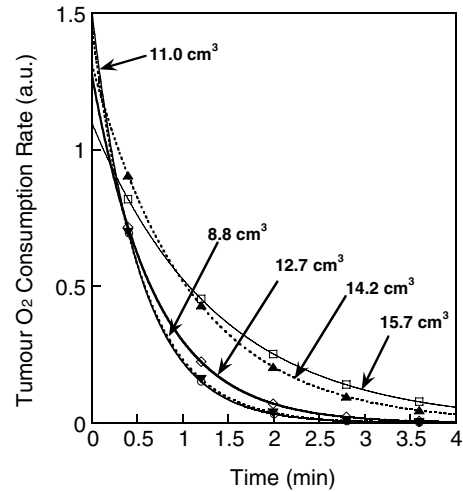


Figure 5. Relationships between the tumour oxygen consumption rates, $|\dot{V}\text{O}_2|$, as a function of time and tumour volume.

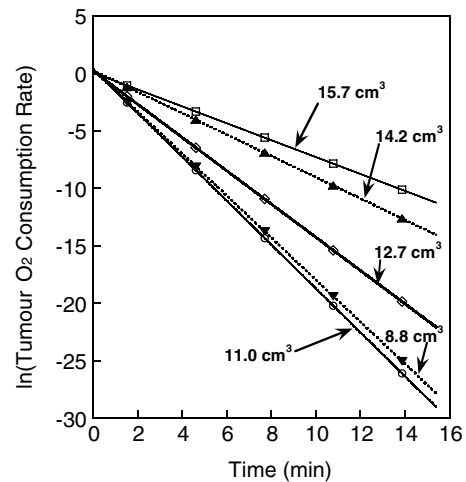


Figure 6. Relationship between tumour oxygen consumption rates, $|\dot{V}\text{O}_2|$, as a function of time and tumour volume plotted on a semilog scale.

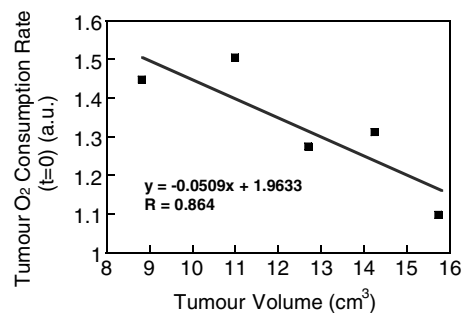


Figure 7. Relationship between tumour oxygen consumption rate at $t = 0$, $|\dot{V}\text{O}_2(0)|$ and tumour volume.

a strong ($R = 0.86$) inverse linear relationship between $\dot{V}\text{O}_2(0)$ and tumour volume, indicating clearly that the larger the tumour, the smaller is its oxygen consumption rate. Furthermore, figure 8 shows the relationship between the mean tumour oxygen consumption rate $\dot{V}\text{O}_2$ and tumour volume after the KCl injection. Again a significant correlation was

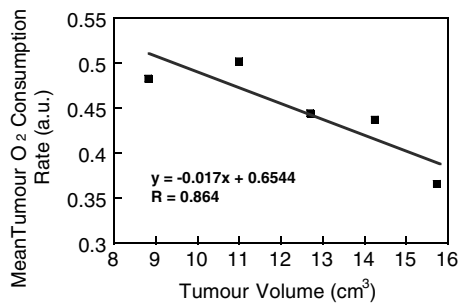


Figure 8. Relationship between the mean tumour oxygen consumption rate $|\dot{V}O_2|$ and tumour volume after KCl injection.

found ($R = 0.86$), suggesting that on average the tumour oxygen consumption rate decreases with an increase in tumour volume.

5. Discussions and conclusion

We developed a mathematical model for computing the oxygen consumption rate in tumours and used NIRS to investigate the oxygen dynamics during KCl-induced cardiac arrest. Although the procedure was invasive, we did not add additional invasiveness for the animal experiment since the NIR readings in the study were taken during the final animal euthanasia. In this way, we could obtain extra and useful physiological parameters, leading to quantification of the tumour oxygen consumption rate. Of course, this methodology has no relevance in human studies, but the knowledge gained here can be useful in understanding solid tumour physiology and is highly relevant for future improvements in tumour treatment.

The NIR signal has been found to be very sensitive to changes in tissue oxygenation in small blood vessels such as arterioles, capillaries and venules [41–44]. These are the places where the oxygen is consumed by tumour/tissue cells. In this study, Fick's Law was applied to extract and quantify the tumour oxygen consumption from the tumour oxygenation dynamics, since the rats died rapidly so that the tumour metabolism or oxygen consumption was not coupled to the tumour blood flow. The overall shapes of the $\Delta[\text{HbO}_2]$ curves, as seen in figures 2(a) and (b), were similar to those obtained by Steen *et al* [27], who used subcutaneously implanted rat 9L gliosarcoma and pentobarbital overdose. Time constant analysis showed that the time constant of oxygenation, τ , determined here was of the same order as reported by Steen *et al*, and that τ was related to tumour oxygen consumption. Moreover, the observation that the magnitude of the drop in $\Delta[\text{Hb}]_{\text{total}}$ was much less than that in $\Delta[\text{HbO}_2]$ may indicate that the decrease in rat tumour $\Delta[\text{HbO}_2]$ was caused mainly by tumour oxygen consumption rather than by a decrease in total tumour blood volume.

We noted that tumour $[\text{HbO}_2]_0$ and tumour volume have a strong, positive linear relationship, as given in figure 3. This correlation makes sense, intuitively, because it simply manifests the fact that the larger the tumour, the more oxygenated haemoglobin is included in the tumour volume. The positive linear relationship between the mean lifetime (τ) and tumour volume (figure 4) indicates that, on average, the time that an

oxyhaemoglobin molecule is likely to survive before it is dissociated to yield a deoxyhaemoglobin molecule and four free oxygen molecules increases with increasing tumour volume. The close correlation between τ and tumour volume suggests that tumour blood perfusion is becoming increasingly poor as the tumour increases in size, leading to increased tumour hypoxia with increasing tumour volume.

As shown in equation (20), the tumour oxygen consumption rate $\dot{V}O_2$ is an exponential function of t and is dependent on both the initial tumour oxyhaemoglobin concentration $[\text{HbO}_2]_0$ and the time constant τ . This means that the tumour oxygen consumption rate $\dot{V}O_2$ decreases exponentially with time after KCl administration. This phenomenon may be explained as follows: as oxygen is being depleted by tumour cellular metabolism, the oxygen concentration or oxygen tension (pO_2) gradient across tumour capillaries and tissues decreases. Since oxygen diffusion is linearly proportional to its concentration gradient according to Fick's Law of diffusion, a lower oxygen concentration gradient or a lower oxygen tension gradient results in decreased oxygen diffusion and thus, less oxygen is available for tumour cellular aerobic respiration. This, in turn, results in less oxygen consumption. This is consistent with several studies, which have reported that oxygen consumption is proportional to the concentration of available oxyhaemoglobin [25, 45–48]. Also, a negative linear relationship between the mean tumour oxygen consumption rate $\dot{V}O_2$ and tumour volume (figure 8) has been observed, consistent with previous reports [49, 50] that larger tumours have lower oxygen consumption. This might be attributed to larger necrotic fraction.

As mentioned in section 1, there are numerous developments and methodologies to quantify tissue oxygen consumption or consumption rate for skeletal muscles [14–18] and for neuronal activities in the brain [19–22], using either experimental or theoretical approaches. But those approaches need to be modified accordingly in order to be suitable for determination of the tumour oxygen consumption rate. The newly developed models for tissue oxygen consumption are relatively complex [23–25], without quantitative association between the tumour consumption rate and the measured NIR haemodynamic parameters. Our study reported in this paper fulfils the need to develop a simplified mathematical model for extracting the tumour oxygen consumption rate from the NIR measurement. While our model is promising, it needs to be validated in our future studies. One of the existing 'gold standard' methods to validate tissue oxygen consumption is to employ a standard Clark oxygen electrode to measure partial oxygen pressure [51]. This method is invasive so it is difficult to be utilized in human studies, but relatively easier in animal tumour studies [10, 28]. The advantage of using the Clark oxygen electrode is mainly to provide absolute values of tissue oxygen consumption readings, while it detects only the local area, perturbs local tissue vasculature and creates difficulties for repeatable measurements. If our methodology is validated in the future by the Clark oxygen electrode, some of the disadvantages of oxygen electrodes can be overcome by the NIR approach. Moreover, since our current method uses relative $\Delta[\text{HbO}_2]$ without the specific values of tumour DPF, the calculated tumour oxygen consumption rate in this paper can be treated more appropriately as a tumour oxygen

consumption index. The methodology has the potential to provide absolute quantification of tumour $\dot{V}O_2$ through NIR haemodynamic measurements once we develop a way to obtain tumour DPF.

While this study demonstrates the possibility of evaluating oxygen consumption rates of tumours by NIRS following KCl administration, the animals have to be sacrificed to perform the measurements. However, similar assessment is also possible through local tissue clamping as performed by Steinberg *et al* [52] for renal cell carcinoma in patients prior to resection. It should be possible to estimate the tumour oxygen consumption rate without sacrificing rats, if we could quantify the blood in-flow and out-flow of the tumours. This might be achieved by introducing a respiratory challenge, such as altering inhaled gas from air to carbogen or oxygen. Indeed, the time course of $\Delta[\text{HbO}_2]$ after KCl administration is not unlike that observed in switching from hyperoxic gas breathing to air as we have reported previously for rat breast and prostate tumours [12, 13, 29] or observed using blood oxygen level dependant (BOLD) contrast proton MRI [53, 54]. It is also similar to the measurements of tissue pO_2 observed in a perfused rat heart in response to induction of total global ischemia [55].

We have used a single channel NIRS in this study, which provides us with global and mean values of the tumour oxygen consumption rate. Using a multi-channel NIRS will allow intratumoural heterogeneity to be investigated and we are currently developing such a capability [56]. Indeed, others have reported spatially resolved NIRS for clinical applications to breast tumours [6, 57]. Once the NIR imaging approach is taken by employing multiple sources and detectors for the measurement, imaging reconstruction algorithms allow us to resolve and detect the tumours that are not superficial [6, 8, 58–61].

In summary, the tumour oxygen consumption rate was calculated by fitting the newly developed model to the measured $\Delta[\text{HbO}_2]$ data. A strong negative linear relationship was found between the mean tumour oxygen consumption rate and tumour volume, indicating that larger tumours have smaller mean oxygen consumption rates. This study further demonstrates the utility of NIRS as an effective, real-time means to investigate the tumour oxygen consumption rate, while further developments are required to make it non-invasive in the future.

Acknowledgments

Supported in part by the Department of Defense Breast Cancer Pre-doctoral Research Fellowships BC962357 (YS), Breast Cancer Initiative IDEA award DAMD17-00-1-0459 (HL) and Cancer Imaging Program NIH P20 CA086354 (RPM). We thank Dr Anca Constantinescu for technical assistance.

References

- [1] Brown J M and Giaccia A J 1998 The unique physiology of solid tumors: opportunities (and problems) for cancer therapy *Cancer Res.* **58** 1408–16
- [2] Höckel M, Schlenger K, Aral B, Mitze M, Schäffer U and Vaupel P 1996 Association between tumor hypoxia and malignant progression in advanced cancer of the uterine cervix *Cancer Res.* **56** 4509–15
- [3] Höckel M and Vaupel P 2001 Tumor Hypoxia: definitions and current clinical, colicig, and molecular aspects *J. Natl Cancer Inst.* **93** 266–76
- [4] Tromberg B, Shah N, Lanning R, Cerussi A, Espinoza J, Pham T, Svaasand L and Butler J 2000 Non-invasive *in vivo* characterization of breast tumors using photon migration spectroscopy *Neoplasia* **2** 26–40
- [5] Fantini S, Walker S A, Franceschini M A, Kaschke M, Schlag P M and Moesta K T 1998 Assessment of the size, position, and optical properties of breast tumors *in vivo* by noninvasive optical methods *Appl. Opt.* **37** 1982–9
- [6] McBride T O, Pogue B W, Jiang S, Österberg U L and Paulsen K D 2001 Initial studies of *in vivo* absorbing and scattering heterogeneity in near-infrared tomographic breast imaging *Opt. Lett.* **26** 822–4
- [7] Hull E L, Conover D L and Foster T 1999 Carbogen-induced changes in rat mammary tumour oxygenation reported by NIR spectroscopy *Br. J. Cancer* **79** 1709–16
- [8] Cheng X F, Mao J M, Bush R, Kopans D B, Moore R H and Chorlton M 2003 Breast cancer detection by mapping hemoglobin concentration and oxygen saturation *Appl. Opt.* **42** 6412–21
- [9] Cheung C, Culver J P, Takahashi K, Greenberg J H and Yodh A G 2001 *In vivo* cerebrovascular measurement combining diffuse near-infrared absorption and correlation spectroscopies *Phys. Med. Biol.* **46** 2053–65
- [10] Menon C *et al* 2003 An integrated approach to measuring tumor oxygen status using human melanoma xenografts as a model *Cancer Res.* **63** 7232–40
- [11] Pogue B W, Paulsen K D, O'Hara J A, Wilmot C M and Swartz H M 2001 Estimation of oxygen distribution in RIF-1 tumors by diffusion model-based interpretation of pimonidazole hypoxia and Eppendorf measurements *Radiat. Res.* **155** 15–25
- [12] Kim J G, Song Y, Zhao D, Constantinescu A, Mason R P and Liu H 2003 Interplay of tumor vascular oxygenation and pO_2 in tumors using NIRS, 19F MR pO_2 mapping, and pO_2 needle electrode *J. Biomed. Opt.* **8** 53–62
- [13] Gu Y, Bourke V, Kim J G, Constantinescu A, Mason R P and Liu H 2003 Dynamic response of breast tumor oxygenation to hyperoxic respiratory challenge monitored with three oxygen-sensitive Parameters *Appl. Opt.* **42** 2960–7
- [14] De Blasi R A, Cope M, Elwell C, Safoue F and Ferrari M 1993 Noninvasive measurement of human forearm oxygen consumption by near-infrared spectroscopy *Eur. J. Appl. Physiol.* **67** 20–5
- [15] De Blasi R A, Ferrari M, Natali A, Conti G, Mega A and Gasparetto A 1994 Noninvasive measurement of forearm blood flow and oxygen consumption by near-infrared spectroscopy *J. Appl. Physiol.* **76** 1388–92
- [16] Homma S, Eda H, Ogasawara S and Kagaya A 1996 Near-infrared estimation of O_2 supply and consumption *J. Appl. Physiol.* **80** 1279–84
- [17] Binzoni T, Quaresima V, Barattelli G, Hiltbrand E, Gürke L, Terrier F, Cerretelli R and Ferrari M 1998 Energy metabolism and interstitial fluid displacement in human gastrocnemius during short ischemic cycles *J. Appl. Physiol.* **85** 1244–51
- [18] Casavola C, Paunescu L A, Fantini S and Gratton E 2000 Blood flow and oxygen consumption with near-infrared spectroscopy and venous occlusion: spatial maps and the effect of time and pressure of inflation *J. Biomed. Opt.* **5** 269–76
- [19] Ferrari M, Mottola L and Quaresima V 2004 Principles, techniques, and limitations of NIR spectroscopy *Can. J. Appl. Physiol.* **29** 463–87
- [20] Sheth S A, Nemoto M, Guiou M, Walker M, Pouratian N and Toga A W 2004 Linear and nonlinear relationships between neuronal activity, oxygen metabolism, and hemodynamic responses *Neuron* **42** 347–55
- [21] Boas D A, Dale A M and Franceschini M A 2004 Diffuse optical imaging of brain activation: approaches to

- optimizing image sensitivity, resolution, and accuracy *NeuroImage* **23** S275–88
- [22] Culver J P, Durduran T, Furuya T, Cheung C, Greenberg J H and Yodh A G 2003 Diffuse optical tomography of cerebral blood flow, oxygenation, and metabolism in rat during focal ischemia *J. Cerebr. Blood Flow Metabolism* **23** 911–24
- [23] Fantini S 2002 A haemodynamic model for the physiological interpretation of in vivo measurements of the concentration and oxygen saturation of haemoglobin *Phys. Med. Biol.* **47** N249–57
- [24] Boas D A, Strangman G, Culver J P, Hoge R D, Jaszewski G, Poldrack R A, Rosen B R and Mandeville J B 2003 Can the cerebral metabolic rate of oxygen be estimated with near-infrared spectroscopy *Phys. Med. Biol.* **48** 2405–18
- [25] Dasu A, Toma-Dasu I and Karlsson M 2003 Theoretical simulation of tumour oxygenation and results from acute and chronic hypoxia *Phys. Med. Biol.* **48** 2829–42
- [26] Vaupel P 1997 Vascularization, blood flow, oxygenation, tissue pH, and bioenergetic status of human breast cancer *Oxygen Transport to Tissue XVIII* ed Nemoto and LaManna (New York: Plenum) pp 243–53
- [27] Steen R G, Kitagishi K and Morgan K 1994 In vivo measurement of tumor blood oxygenation by near-infrared spectroscopy: immediate effects of pentobarbital overdose or carmustine treatment *J. Neuro-Oncol.* **22** 209–20
- [28] Kawauchi S, Morimoto Y, Sato S, Arai T, Seguchi K, Asanuma H and Kikuchi M 2004 Differences between cytotoxicity in photodynamic therapy using a pulsed laser and a continuous wave laser: study of oxygen consumption and photobleaching *Laser Med. Sci.* **18** 179–83
- [29] Liu H, Song Y, Worden K L, Jiang X, Constantinescu A and Mason R P 2000 Noninvasive investigation of blood oxygenation dynamics of tumors by near-infrared spectroscopy *Appl. Opt.* **39** 5231–43
- [30] Benesch R, Macduff G and Benesch R E 1965 Determination of oxygen equilibria with a versatile new tonometer *Anal. Biochem.* **11** 81–7
- [31] Benesch R E, Benesch R and Yung S 1973 Equations for the spectrophotometric analysis of hemoglobin mixtures *Anal. Biochem.* **55** 245–8
- [32] van Assendelft O W and Zijlstra W G 1975 Extinction coefficients for use in equations for the spectrophotometric analysis of haemoglobin mixtures *Anal. Biochem.* **69** 43–8
- [33] Fishkin J B, Coquoz O, Anderson E R, Brenner M and Tromberg B J 1997 Frequency-domain photon migration measurements of normal and malignant tissue optical properties in a human subject *Appl. Opt.* **36** 10
- [34] ISS Inc. 2003 Near-infrared, non-invasive tissue oximeter *User Manual USA*
- [35] Sevick E M, Chance B, Leigh J, Nioka S and Maris M 1991 Quantitation of time- and frequency-resolved optical spectra for the determination of tissue oxygenation *Anal. Biochem.* **195** 330–51
- [36] Delpy D T and Cope M 1997 Quantification in tissue near infrared spectroscopy *Phil. Trans. R. Soc. Lond. B* **952** 649–59
- [37] Zijlstra W G, Buursma A and Meeuwse-van der Roest W P 1991 Absorption spectra of human fetal and adult oxyhemoglobin, de-oxyhemoglobin, carboxyhemoglobin, and methemoglobin *Clin. Chem.* **37** 1633–8
- [38] Yang Y, Liu H, Li X and Chance B 1997 A low cost frequency-domain photon migration instrument for tissue spectroscopy, oximetry, and imaging *Opt. Eng.* **36** 1562–9
- [39] Hahn E W, Peschke P, Mason R P, Babcock E E and Antich P P 1993 Isolated tumor growth in a surgically formed skin pedicle in the rat: a new tumor model for NMR studies *Magn. Reson. Imaging* **11** 1007–17
- [40] Kety S S 1987 Cerebral circulation and its measurement by inert diffusible tracers *Israel J. Med. Sci.* **23** 3–7
- [41] Chance B, Dait M T, Zhang C, Hamaoka T and Hagerman F 1992 Recovery from exercise-induced desaturation in the quadriceps muscles of elite competitive rowers *Am. J. Physiol.—Cell Physiol.* **262** C766–75
- [42] Mancini D M, Bolinger L, Liu H, Kendrick K, Chance B and Wilson J R 1994 Validation of near-infrared spectroscopy in humans *J. Appl. Physiol.* **77** 2740–7
- [43] Hampson N B and Piantadosi C A 1988 Near infrared monitoring of human skeletal muscle oxygenation during forearm ischemia *J. Appl. Physiol.* **64** 2449–57
- [44] Liu H, Hielscher A H, Tittel F K, Jacques S L and Chance B 1995 Influence of blood vessels on the measurement of hemoglobin oxygenation as determined by time-resolved reflectance spectroscopy *Med. Phys.* **22** 1209–17
- [45] Vaupel P W Oxygenation of solid tumors *Drug Resistance in Oncology* ed B A Teicher (New York: Dekker) pp 53–85
- [46] Gullino P M, Grantham F H and Courtney A H 1967 Utilization of oxygen by transplanted tumors in vivo *Cancer Res.* **27** 1020–9
- [47] Kristensen C A, Roberge S and Jain R K 1997 Effect of tumor necrosis factor alpha on vascular resistance, nitric oxide production, and glucose and oxygen consumption in perfused tissue isolated human melanoma xenografts *Clin. Cancer Res.* **3** 319–24
- [48] Dewhirst M W, Secomb T W, Ong E T, Hsu R and Gross J F 1994 Determination of local oxygen consumption rates in tumors *Cancer Res.* **54** 3333–6
- [49] Jain R K and Ward-Hartley K 1984 Tumor blood flow: characterization, modification and role in hyperthermia *IEEE Trans. Sonics Ultrasonics* **SU-31** 504–26
- [50] Song C W 1984 Effect of local hyperthermia on blood flow and microenvironment *Cancer Res.* **44** (Suppl.) 4721s–30s
- [51] Lang M A, Rosenthal S J, Caplan S R and Essig A 1979 Measurement of oxygen consumption in voltage-clamped epithelia *Am. J. Physiol.* **236** F206–9
- [52] Steinberg F, Röhrborn H J, Otto T, Scheufler K M and Streffer C 1997 NIR reflection measurements of hemoglobin and cytochrome aa3 in healthy tissue and tumors *Adv. Exp. Med. Biol.* **428** 69–77
- [53] Jiang L, Zhao D, Constantinescu A and Mason R P 2004 Comparison of BOLD contrast and Gd-DTPA dynamic contrast enhanced imaging in rat prostate tumor *Magn. Reson. Med.* **51** 953–60
- [54] Robinson S P, Howe F A and Griffiths J R 1995 Noninvasive monitoring of carbogen-induced changes in tumor blood flow and oxygenation by functional MRI *Int. J. Radiat. Oncol. Biol. Phys.* **33** 855–9
- [55] Mason R P, Jeffrey F M H, Malloy C R, Babcock E E and Antich P P 1992 A noninvasive assessment of myocardial oxygen tension: ¹⁹F NMR spectroscopy of sequestered perfluorocarbon emulsion *Magn. Reson. Med.* **27** 310–17
- [56] Kim J G, Gu Y, Constantinescu A, Mason R P and Liu H 2003 Non-uniform tumor vascular oxygen dynamics monitored by three-channel near-infrared spectroscopy *Proc. SPIE* **4955** 388–96
- [57] Chance B 2002 High sensitivity and specificity in human breast cancer detection with near-infrared imaging *OSA Biomedical Topical Meetings, Technical Digest* pp 450–5
- [58] Hielscher A H, Klose A D and Hanson K M 1999 Gradient-based iterative reconstruction scheme for time-resolved optical tomography *IEEE Trans. Med. Imaging* **18** 262–71
- [59] Yao Y Q, Wang Y, Pei Y L, Zhu W W and Barbour R L 1997 Frequency-domain optical imaging of absorption and scattering distributions by Born iterative method *J. Opt. Soc. Am. A* **14** 325–42
- [60] Paulsen K D and Jiang H 1996 Enhanced frequency domain optical image reconstruction in tissues through total variation minimization *Appl. Opt.* **35** 3447–58
- [61] Schotland J C 1997 Continuous-wave diffusion imaging *J. Opt. Soc. Am.* **14** 275–9